CENTRAL RESEARCH LIBRARY
DOCUMENT COLLECTION

OAK RIDGE NATIONAL LABORATORY
OPERATED BY
UNION CARBIDE CORPORATION
NUCLEAR DIVISION

POST OFFICE BOX X
OAK RIDGE, TENNESSEE 37830

ORNL-MIT-94

DATE: January 28, 1970 COPY NO. 16

SUBJECT: Single-Phase Flow Regimes in a Multistage Flash Evaporator Stage

AUTHOR: J.D. Dearth, T.M. McAuley, and A.M. Sheikh

Consultants: S.J. Ball, N.E. Clapp, Jr., and R.P. Wichner

ABSTRACT

Single-phase flows in a mockup flash evaporator stage were characterized in terms of three possible flow regimes: shooting, jump, or submerged flows. It was found that in the first two regimes liquid flow rates depended only upon upstream liquid level, interstage pressure difference, and orifice opening. These data could be correlated by plotting orifice Froude number versus the ratio of upstream level to orifice opening for constant values of the pressure difference - orifice opening ratio. For submerged flows an additional parameter, the downstream liquid level, was found to be important, and the data for this regime were fitted to a three-variable least-squares quadratic polynomial with a standard error of 4.5%. Analytical correlation of flow rate data was frustrated by uncertainties in the experimental magnitudes of contraction coefficients and energy losses, to which the liquid flow rates were extremely sensitive.

OAK RIDGE NATIONAL LABORATORY
CENTRAL RESEARCH LIBRARY
DOCUMENT COLLECTION
LIBRARY LOAN COPY
DO NOT TRANSFER TO ANOTHER PERSON
If you wish someone else to see this document, send in name with document and the library will arrange a loan.

Oak Ridge Station
School of Chemical Engineering Practice
Massachusetts Institute of Technology

[redacted]

Contents

1. SUMMARY

Because of the potential application of multistage flash evaporators in nuclear-powered desalination plants, efforts are currently being made at ORNL to understand and improve their operation. Experimental and theoretical work has indicated that the stability of a large MSF plant is extremely sensitive to interphase flow conditions, but the complexity of open-channel flow with flashing has hindered the development of mathematical models for controls studies.

The approach to this problem involves the correlation of data for single-phase flows, in the hope that corrections for the effects of flashing may eventually be applied. The objectives of this study were to define the important regimes of single-phase flow in a typical stage, to determine the important system parameters which affect interstage flow rates, and to correlate flow rates in terms of the important system variables.

Flow characterization experiments carried out in an 8-ft-long by 1-ft-wide full-scale mockup of a flashing stage indicated three distinct regimes of flow: "shooting flow," with no liquid seal at the downstream orifice; "jump flow," with a hydraulic jump occurring at some intermediate point on the stage; and "submerged flow," with a liquid level behind the inlet orifice greater than the orifice opening. In the first two regimes liquid flow from the orifice was supercritical and non-submerged, so that downstream levels and velocities had no influence upon liquid flow rates. In the third regime the downstream level affected the rate of flow through the first orifice.

Flow rates in the non-submerged regimes were correlated using the dimensionless quantities q^2/gB^3, L_1/B, and $\Delta P_v/B$. This three-parameter relationship was conveniently represented in graphical form. In the submerged regime an additional variable, L_2/B, made graphical representation impractical; instead data were fitted to a three-variable least-squares polynomial expression with a standard error of 4.5% in the predicted Froude number. Development of analytical expressions for flow rate was frustrated by the extreme sensitivity of the flow relations to contraction coefficient and energy loss across the orifice, neither of which could be accurately measured or predicted.

2. INTRODUCTION

Although multistage flash evaporators have been in use for many years, few fundamental studies of their operation have been conducted. Because of their potential application in nuclear-powered desalination plants, methods of improving their operation are currently under investigation at ORNL. Experimental observations and simulation studies have indicated that the stability of large multistage flash plants is extremely sensitive to flow conditions, and particularly to the effect of downstream brine levels.

Development of accurate theoretical flow models for control studies has been hindered by the complexity of open-channel hydraulics, and existing relations for the flow of submerged jets have proven inadequate in accounting for the effects of flashing and interstage pressure differences. Empirical flow correlations developed thus far have suffered from the disadvantages of poor scaleup and inaccurate flow rate prediction outside the range of experimental data (2).

The current research effort is directed towards the characterization of single-phase flows, in the hope that the relations obtained may be corrected for the effects of flashing. The objectives of the current study were as follows:

1. Definition of the different regimes of single-phase flow.

2. Determination of the important system parameters which affect interstage flow rates.

3. Correlation of flow rates as functions of the important parameters.

The method of attack involved an integrated program of experimental and theoretical studies. Parameters such as liquid rates, orifice settings, and interstage pressure differences were varied and the resulting flow regimes were observed. Based on these preliminary observations and a survey of the literature, tentative models were formulated and a systematic variation of the important variable-groupings was carried out to determine their effects upon flow rates. Supplementary investigations utilized a traversing pitot tube to characterize velocity profiles and provide information relevant to the mathematical modeling of the flow processes.

3. APPARATUS AND PROCEDURE

Flow studies were carried out in an 8-ft-long by 1-ft-wide full-scale mockup of a flashing stage shown in Fig. 1. A portion of one side was constructed of clear plastic to allow direct observation of the flow. The heights of both the inlet and outlet orifices were adjustable from 0 to 13 in. An entrance region upstream of the first orifice was sealed and could be pressurized to allow an interstage pressure drop up to 10 in. of water.

The stage mockup completed a water circulation loop consisting of a 300-gal surge tank, a centrifugal pump with a 100-hp motor, and piping. The circulation system had a maximum capacity of 0.75×10^6 lb of water/hr. Liquid flow through the device was controlled by an adjustable bypass valve between the discharge and suction of the pump and a valve immediately before the test stage. The flow rate was measured by an orifice meter in the liquid line.

The mockup stage was equipped with sight glasses to measure the liquid levels 12 in. upstream from the first orifice, 9-1/4 in. and 42 in. downstream of the first orifice and 12 in. upstream of the second orifice. The

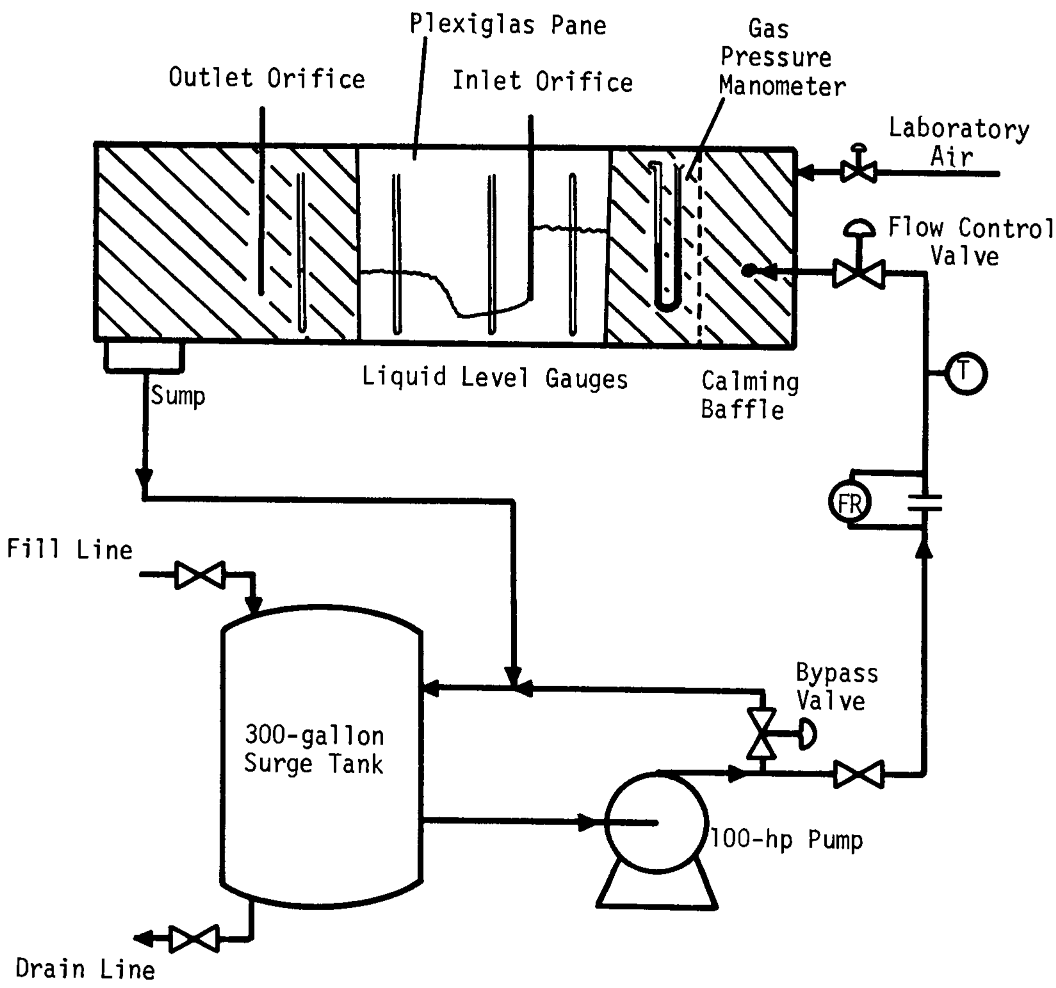

MASSACHUSETTS INSTITUTE OF TECHNOLOGY
SCHOOL OF CHEMICAL ENGINEERING PRACTICE
AT
OAK RIDGE NATIONAL LABORATORY

Diagram of Flowbox Apparatus

DATE	DRAWN BY	FILE NO.	FIG.
1-26-70	TMM	CEPS-X-94	1

interstage air pressure difference was measured by a water-filled manometer. A movable pitot-type probe was used to measure local liquid velocities.

Before a series of runs was made, the circulation system was filled until the desired level was reached in the test stage (between 10 and 15 in.). The water feed was then reduced to a flow which compensated for leaks in the system.

The first regime of flow investigated was the case of non-submerged flow. Since flow from the orifice was always supercritical, downstream conditions would not have an effect on upstream flow. Dimensional analysis and energy conservation considerations indicated that the liquid flow rate should be a function of the liquid head before the inlet orifice, any interstage pressure drop, and the orifice opening (see Sect. 9.1.1.1). Data were taken to determine the relationship for several liquid flow rates. The orifice heights were adjusted to give non-submerged flow in the test stage. The liquid levels in the test stage were measured by the sight glasses. Additional data were taken with an interstage pressure drop.

If the downstream orifice restricts the flow out of the stage sufficiently, the upstream orifice will become submerged. The jet of rapidly moving water issuing from the upstream orifice will be covered by a mass of liquid with no resultant velocity. This condition has been analyzed by Henry (6), assuming energy is conserved by the liquid as it passes through the orifice and momentum is conserved as the jet diffuses. Investigations (1, 4) have found that the analysis of Henry does not work well for the situation under study.

As in the non-submerged case, the inlet orifice, liquid head upstream of the orifice and interstage pressure drop are significant. Since the flow from the orifice is submerged, downstream conditions influence the flow, and downstream liquid level and depth of submergence become important parameters (see Sect. 9.1.2.1).

Data were obtained to determine the relationship of flow rate to the above parameters. For a series of liquid flows, the ratio of downstream liquid level to inlet orifice was maintained constant by adjusting the outlet orifice. All other liquid levels were then measured.

Knowledge of the size and location of the vena contracta of the submerged jet was necessary for correlating data and checking energy and momentum balances. This information was obtained by traversing the flow with a pitot tube probe. The location of the vena contracta was found by moving the probe upstream at a distance of about 3 in. from the bottom along the centerline of the channel until the liquid velocity reached a maximum. A velocity profile measured at this location indicated the size of the jet.

4. RESULTS

4.1 Flow Characterization

Flow characterization experiments indicated that the single-phase flows in our experimental stage could be grouped into three regimes. These are illustrated in Figs. 2 and 3 and are described in detail below.

The shooting flow regime was characterized by the absence of a liquid seal at the downstream orifice. Liquid leaving the inlet orifice at supercritical velocities (7) was observed to "shoot" across the bottom of the test stage in a narrow stream and to pass underneath the second orifice.

The jump flow regime was characterized by the occurrence of a hydrulic jump between the supercritical liquid leaving the inlet orifice and the subcritical liquid approaching the exit orifice. The location of the jump was influenced by the liquid flow rate, orifice settings, interstage pressure difference, and liquid inventory as shown in Table 1.

Table 1. Effect of Operating Variables on Jump Position

Increase In	Direction of Jump Movement
Liquid flow rate	Downstream
Interstage pressure difference	Upstream
Upstream orifice opening	Upstream
Liquid inventory	Upstream
Downstream orifice opening	Downstream

The submerged flow regime was characterized by a liquid level on the downstream side of the inlet orifice greater than the height of the orifice opening. Observation of flow patterns of entrained bubbles led to the conclusion that a sharp graduation in velocities existed between the nearly-stagnant liquid near the free surface and the fast-moving jet emerging from the orifice.

The transition from jump flow to shooting flow was observed at the outlet orifice with no vapor-phase pressure difference. A more realistic situation occurs when shooting flow takes place through an orifice with a pressure drop across it. This situation was produced with the first orifice by increasing the pressure on the upstream side of the orifice until the upstream liquid level fell below the bottom of the weir. When vapor

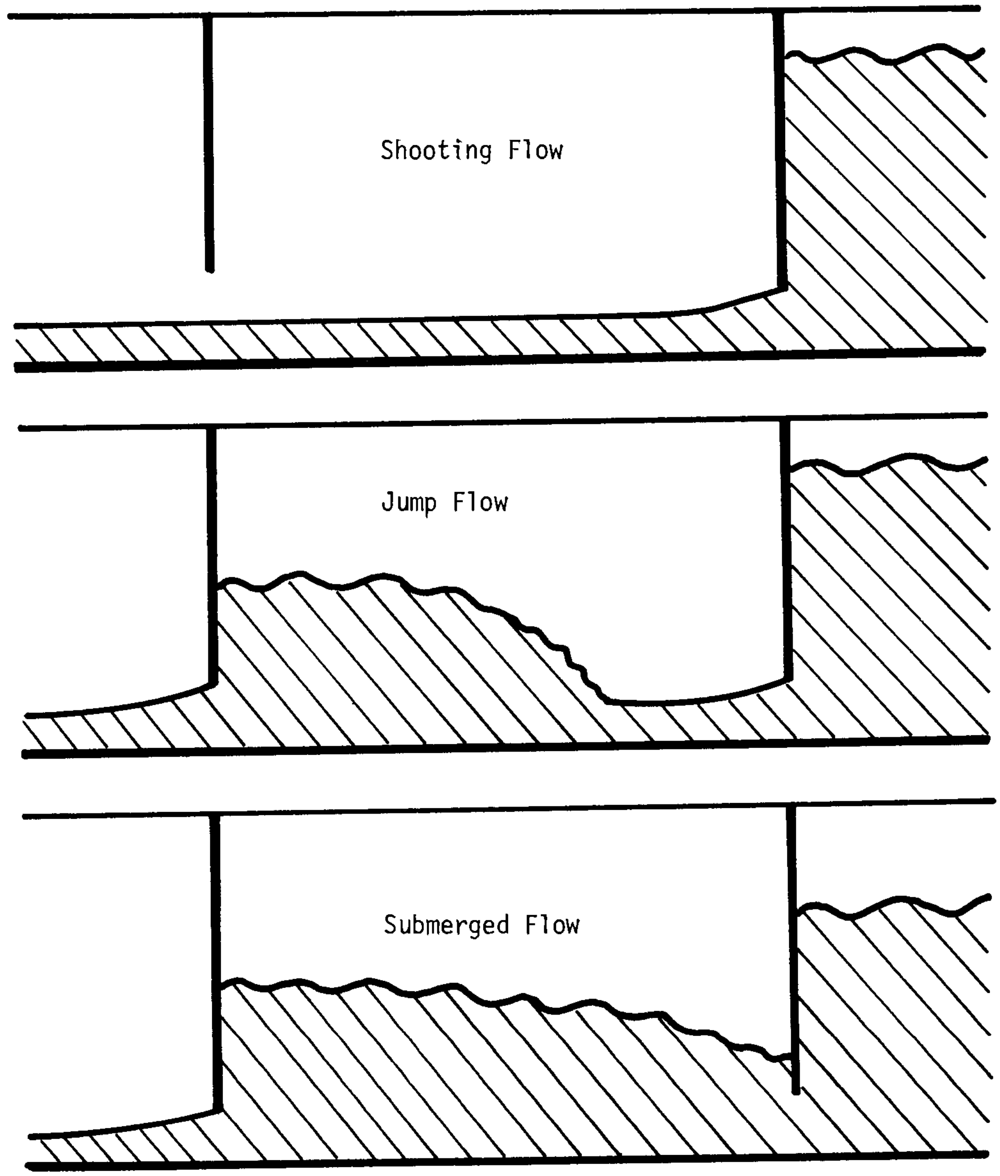

MASSACHUSETTS INSTITUTE OF TECHNOLOGY
SCHOOL OF CHEMICAL ENGINEERING PRACTICE
AT
OAK RIDGE NATIONAL LABORATORY

Flow Regimes Observed in MSF Evaporator Test Stage

DATE	DRAWN BY	FILE NO.	FIG.
1-27-70	TMM	CEPS-X-94	2

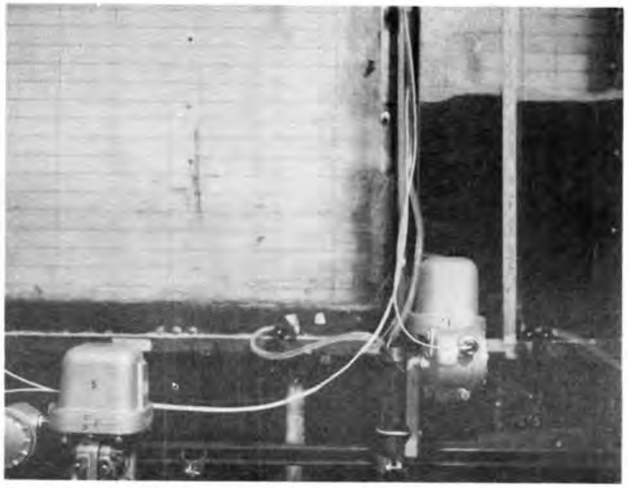

3a. Shooting Flow

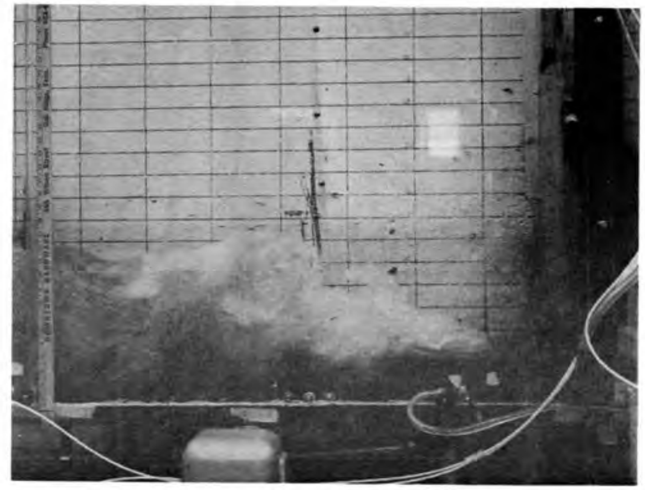

3b. Hydraulic Jump

MASSACHUSETTS INSTITUTE OF TECHNOLOGY SCHOOL OF CHEMICAL ENGINEERING PRACTICE AT OAK RIDGE NATIONAL LABORATORY			
Photographic Description of Flow Regimes			
DATE 1-28-70	DRAWN BY AMS	FILE NO. CEPS-X-94	FIG. 3

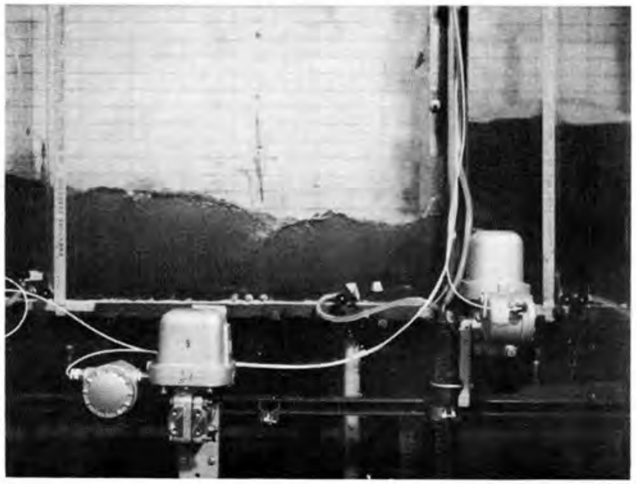

3c. Submerged Flow

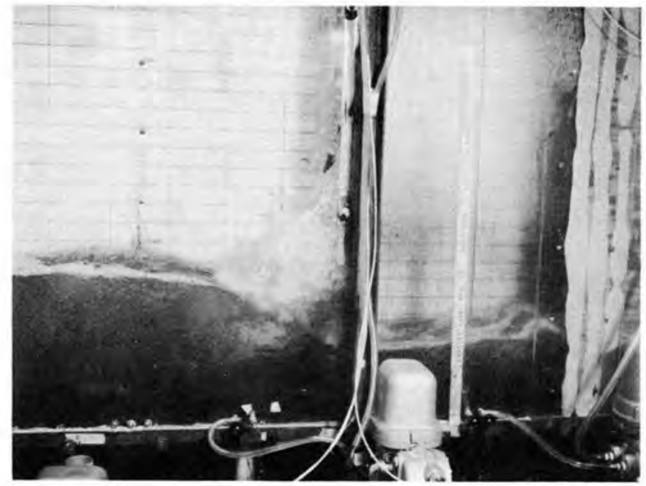

3d. Blow-Through

MASSACHUSETTS INSTITUTE OF TECHNOLOGY SCHOOL OF CHEMICAL ENGINEERING PRACTICE AT OAK RIDGE NATIONAL LABORATORY			
Photographic Description of Flow Regimes			
DATE 1-28-70	DRAWN BY AMS	FILE NO. CEPS-X-94	FIG. 3

blow-through occurred, the gas pressure on the upstream side decreased, causing the upstream liquid level to rise and reseal the bottom of the weir. Sealing the weir with liquid prevented vapor flow, resulting in an increased upstream pressure which forced the liquid level down once again. The system was observed to oscillate with gas pressures of 2 to 10 in. of water and about a 1-sec period, for one of the sets of conditions investigated. Figure 3d shows the effect of blow-through when the downstream side of the orifice is submerged.

The transition from jump flow to submerged flow was observed to occur somewhat less dramatically. The hydraulic jump migrated upstream until it reached the inlet orifice, at which point the liquid level just downstream of the orifice began to increase and submergence was obtained. The submergence process did involve the formation of large (2 to 3 in. amplitude) waves just downstream of the orifice; these were damped out as liquid depth was increased.

4.2 Flow Rate Correlations

For non-submerged flows dimensional analysis indicated that it should be possible to correlate the Froude number, q^2/gB^2, as a function of the dimensionless ratios L_1/B and $\Delta P_V/B$ (see Appendix 9.6 and Fig. 9 for nomenclature). Data taken for fixed values of the ratio $\Delta P_V/B$ = 0, 1/2, 1, and 2 are shown in Fig. 4. Calculated Froude numbers were found to be independent of downstream level L_2 and initial liquid inventory. Experimental values of the contraction coefficient of 0.65 inserted into an energy balance across the orifice predicted Froude numbers about 7% higher than those observed, indicating energy losses of approximately that magnitude. Figure 5 shows velocity profiles measured at the channel centerline immediately before and after a hydraulic jump. (Note that the inlet orifice is on the left-hand side in Fig. 5.) The ratios of the two liquid levels calculated from a momentum balance across the jump checked with the experiment within 3%.

For submerged flow the Froude number is a function of L_1/B, $\Delta P_V/B$, and L_2/B. An empirical least squares fit (Appendix 9.4) to the experimental data of Ball and Clapp (4), using quadratic functions of each of the three independent variables, predicted Froude numbers with a standard error of 4.5%; this implies that q may be predicted within ± 2.2%. The dependence of Froude number upon L_1/B, L_2/B, and $\Delta P_V/B$ is illustrated in Figs. 6 and 7.

Pitot tube velocity profiles for submerged flow are shown in Fig. 8. The location of the submerged vena contracta was found to be about one orifice opening downstream from the weir. Six vertical centerline traverses at the vena contracta for different Froude numbers and t'/B ratios permitted calculation of equivalent contraction coefficients for use in both energy and momentum balance relations as follows:

1) From an energy balance:

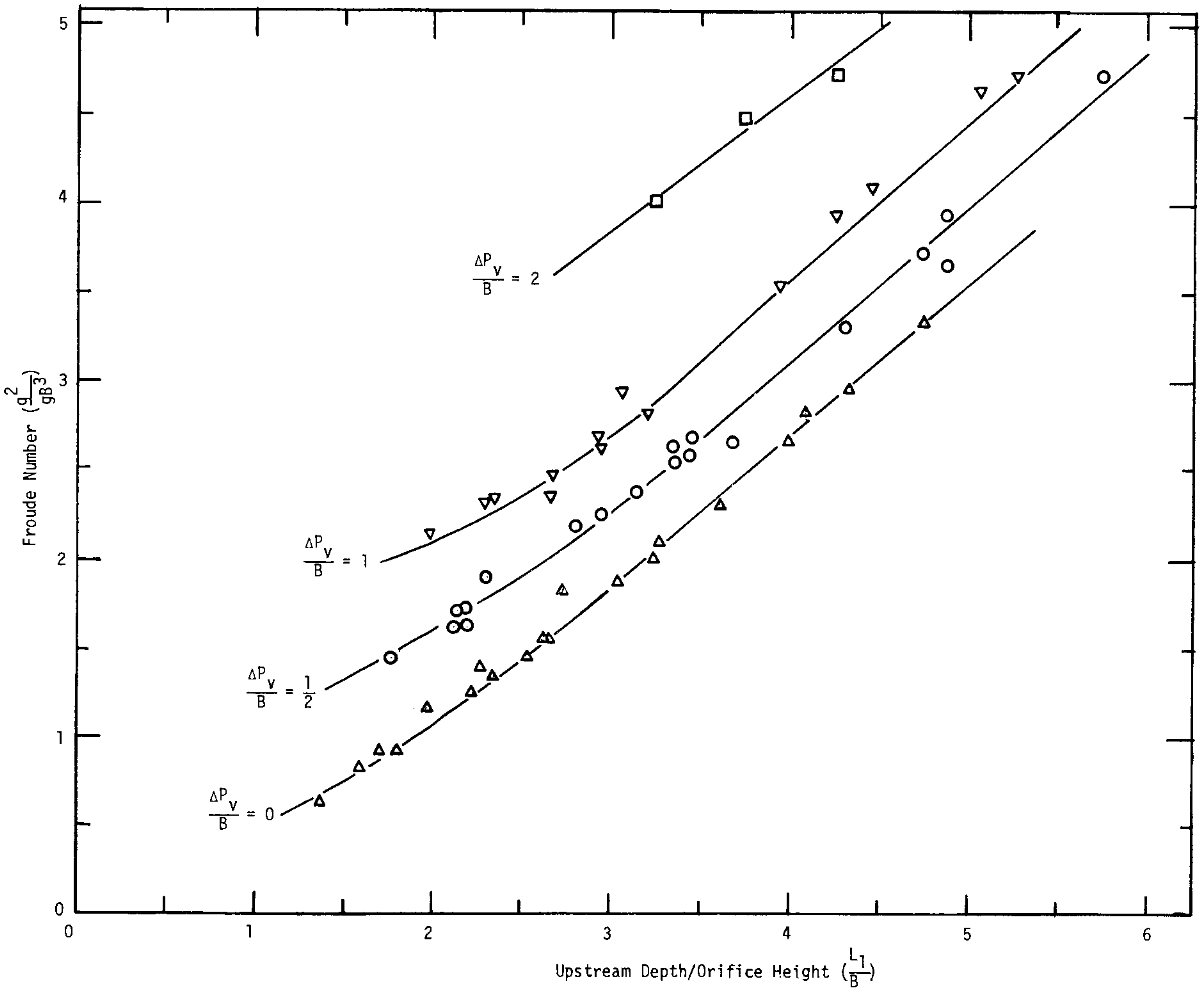

MASSACHUSETTS INSTITUTE OF TECHNOLOGY
SCHOOL OF CHEMICAL ENGINEERING PRACTICE
AT
OAK RIDGE NATIONAL LABORATORY

Flow Rate Correlation for Non-Submerged Flow

DATE	DRAWN BY	FILE NO.	FIG.
1-27-70	AMS	CEPS-X-94	4

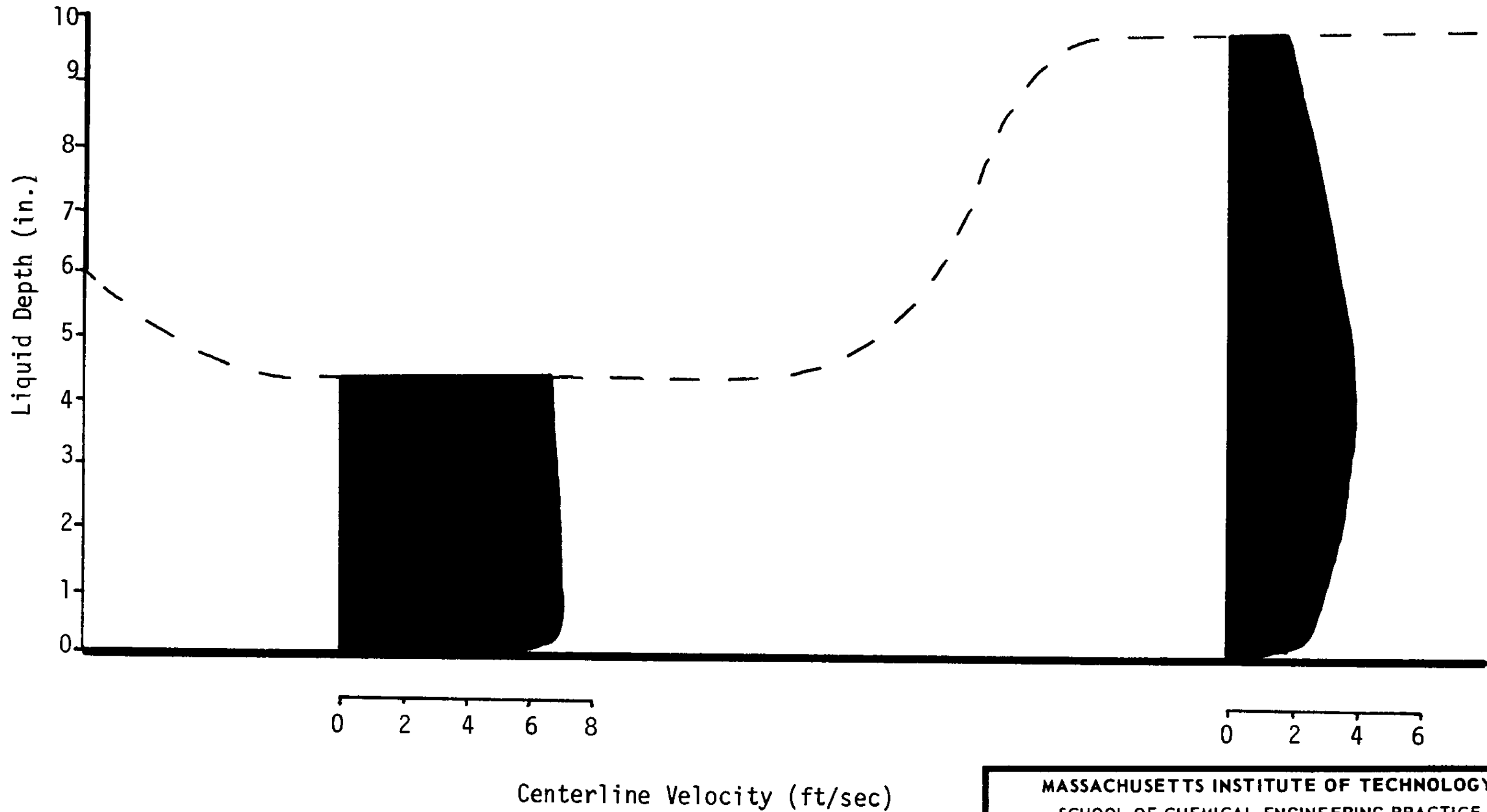

MASSACHUSETTS INSTITUTE OF TECHNOLOGY
SCHOOL OF CHEMICAL ENGINEERING PRACTICE
AT
OAK RIDGE NATIONAL LABORATORY

Jump Flow Velocity Profiles

DATE	DRAWN BY	FILE NO.	FIG.
1-26-70	TMM	CEPS-X-94	5

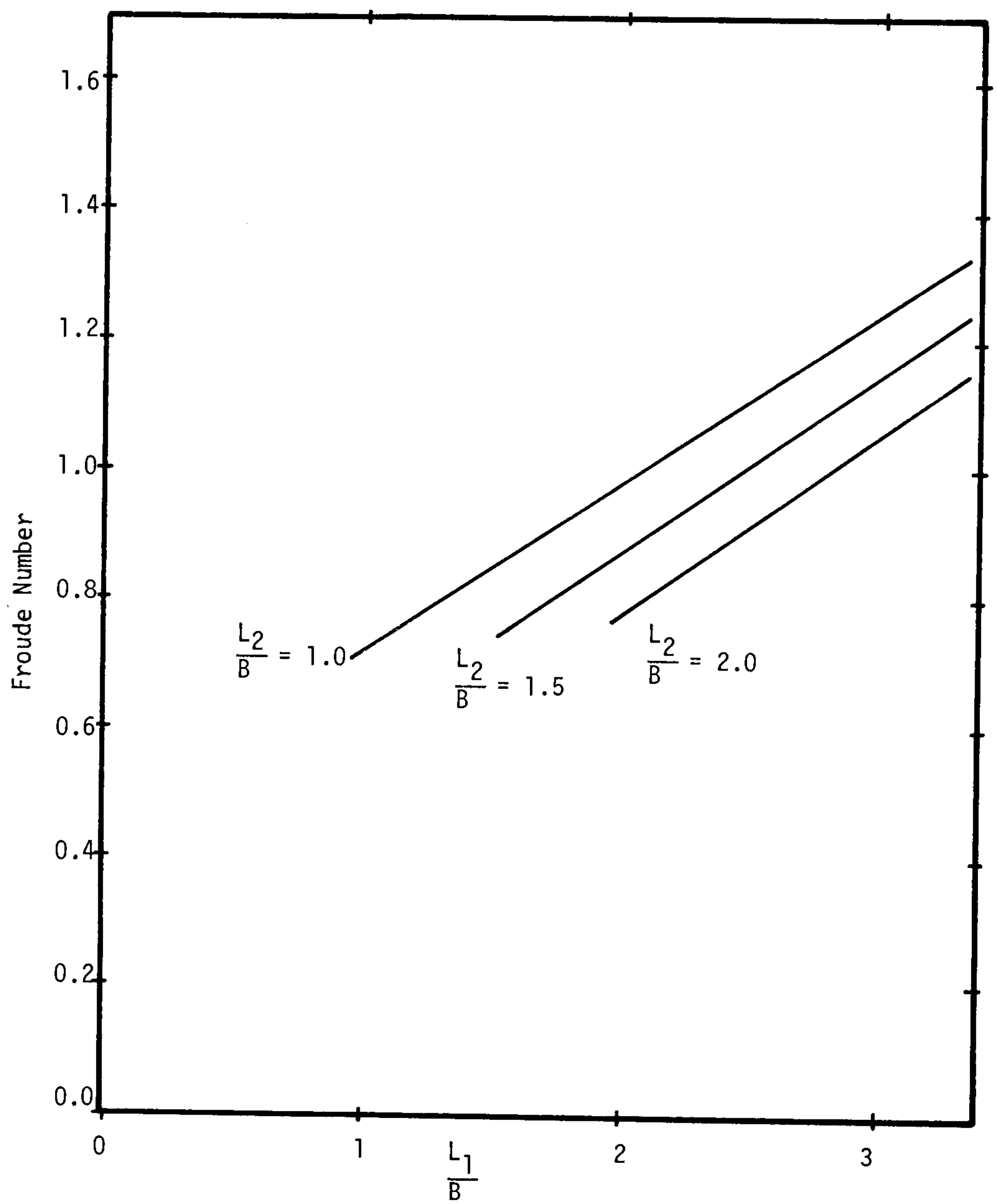

MASSACHUSETTS INSTITUTE OF TECHNOLOGY
SCHOOL OF CHEMICAL ENGINEERING PRACTICE
AT
OAK RIDGE NATIONAL LABORATORY

Empirical Correlation for Submerged Flow, $\Delta P_V/B = 0.0$

DATE	DRAWN BY	FILE NO.	FIG.
1-28-70	TMM	CEPS-X-94	6

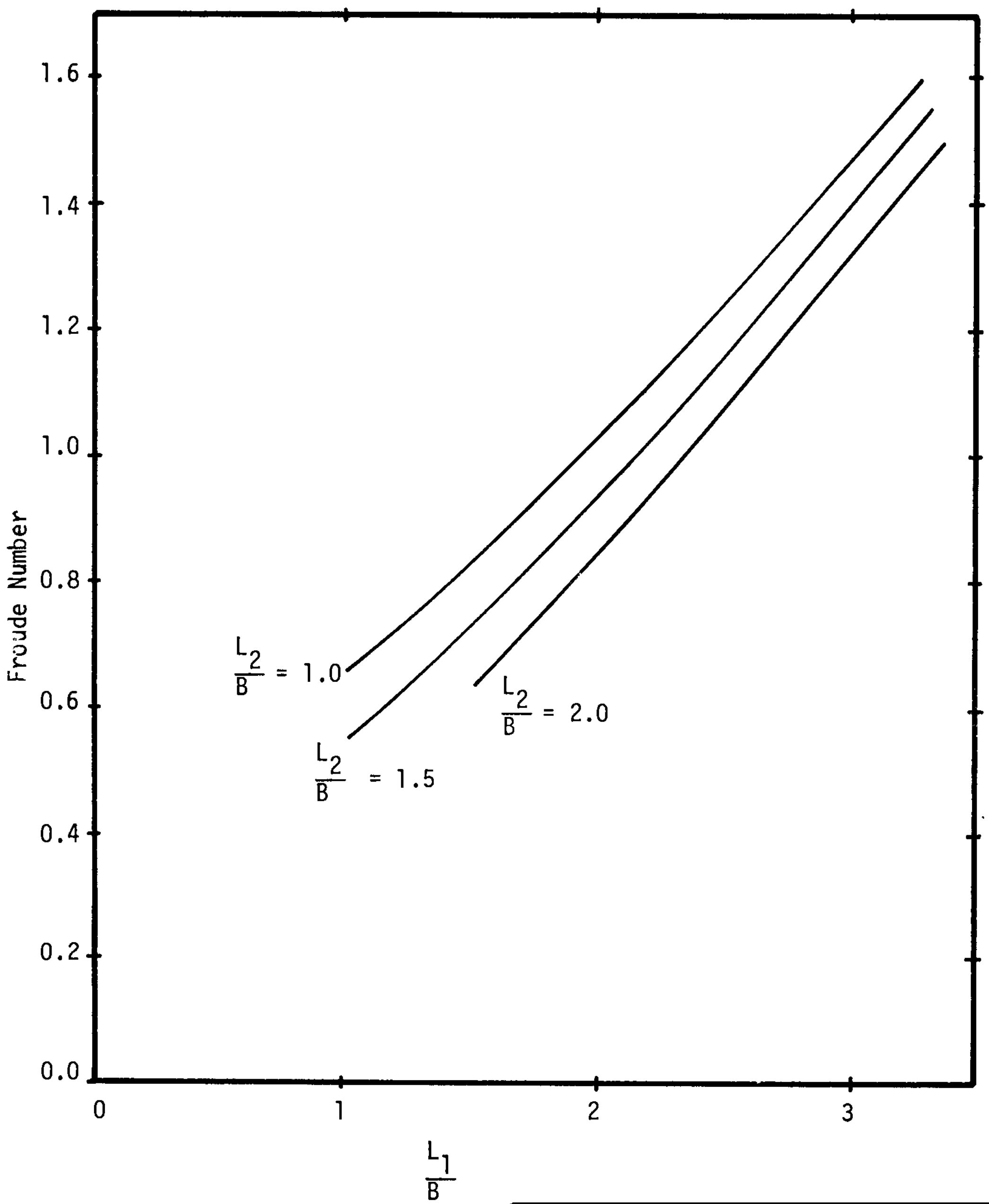

MASSACHUSETTS INSTITUTE OF TECHNOLOGY
SCHOOL OF CHEMICAL ENGINEERING PRACTICE
AT
OAK RIDGE NATIONAL LABORATORY

Empirical Correlation for Submerged Flow, $\Delta P_V/B = 0.5$

DATE	DRAWN BY	FILE NO.	FIG.
1-28-70	TMM	CEPS-X-94	7

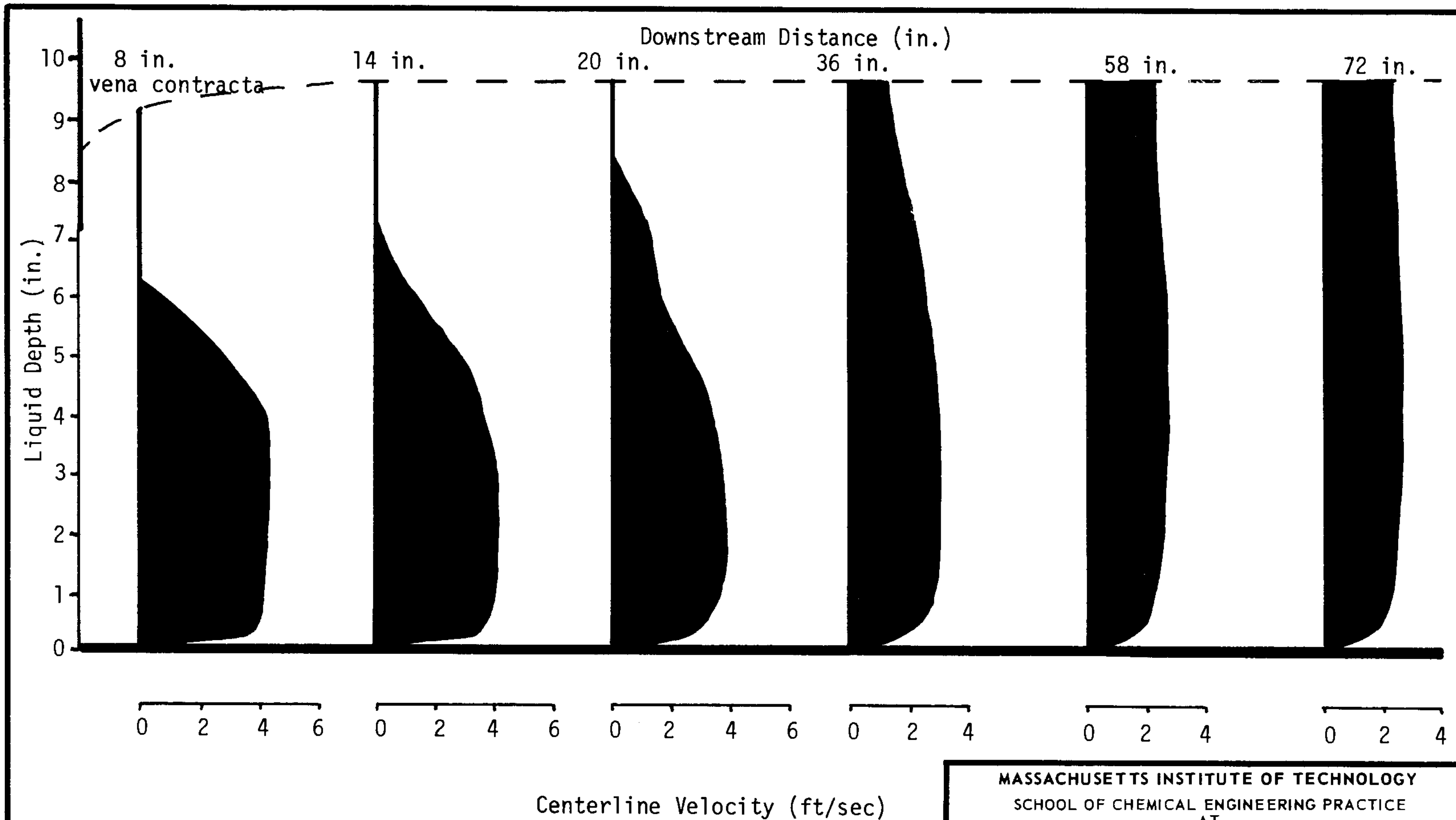

MASSACHUSETTS INSTITUTE OF TECHNOLOGY
SCHOOL OF CHEMICAL ENGINEERING PRACTICE
AT
OAK RIDGE NATIONAL LABORATORY

Submerged Flow Velocity Profiles

DATE	DRAWN BY	FILE NO.	FIG.
1-26-70	TMM	CEPS-X-94	8

$$C_c = \sqrt{\frac{q^3}{B^2 \int V^3 \, dy}} = 0.72 \pm 0.05$$

2) From a momentum balance:

$$C_c = \frac{q^2}{B \int V^2 \, dy} = 0.75 \pm 0.07$$

A value of t' calculated from a downstream momentum balance predicted energy losses across the orifice to be about 5% (see Appendix 9.3.1).

5. DISCUSSION OF RESULTS

The occurrence of shooting flow in a practical multistage flash unit appears extremely unlikely due to the oscillatory condition which is established when the upstream liquid level falls below the orifice opening. Moreover, if such a regime did occur, it would be undesirable for the following reasons:

1) When shooting flow occurs, two or more flashing stages are effectively replaced by a single stage, thus decreasing the operating efficiency of the plant.

2) Restoration of the liquid seal is hindered by the oscillatory condition mentioned above, and the disturbance may propagate throughout the plant if an effective control strategy is not adopted.

Because the flows in the shooting regime are non-submerged and supercritical, flow rates may be predicted by use of the same relationships valid in the jump flow regime.

The existence of a hydraulic jump between the inlet and outlet orifices is characteristic of situations where flow from the inlet orifice is supercritical and that approaching the outlet orifice is subcritical. The location of the hydraulic jump is not random, but is dependent upon such factors as stage length, inlet and outlet orifice settings, liquid flow rate, interstage pressure differences, and liquid inventory. The ability to predict the position of the jump is important in determining the prevailing flow regime, and although the limitations of the present experimental apparatus (e.g., end effects, no pressure difference across the exit orifice) prevented investigation of all factors, a theoretical approach to the problem is included in Appendix 9.2.

Jump flow was never observed in our apparatus for orifice Froude numbers, Fr_B, less than 0.5. The theoretical lower limit for occurrence of critical flow at the vena contracta is $Fr_B = C_c^3$, which for a contraction coefficient of 0.65 has the value 0.274. Because flows in excess of the critical have the property that disturbances occurring downstream can have no effect upon flow conditions upstream, the rate of flow through an orifice leading to a stage where jump flow is occurring is a function only of orifice opening, upstream liquid level, and interstage pressure difference. This conclusion is supported by our data (see Fig. 5). The proposed correlation is valid only where the upstream velocity distribution is essentially uniform. The slight upward curvature of the lines of constant $\Delta P_V/B$ for low values of the L_1/B ratio reflects the increased importance of upstream velocity-head at low values of the potential head; the wider separation of the curves is indicative of the fact that $\Delta P_V/B$ makes a greater fractional contribution to the upstream liquid head when L_1/B is small (see Appendix 9.1.1.2).

For submerged flow the analytical expressions derived from considerations of energy and momentum conservation (6) were found to have numerous practical shortcomings. First, it was concluded that contraction coefficients for sluice-gate underflow were not known accurately enough to be used in relations where flow rates depended upon C_c to the 0.5 to 1.0 power. In fact, because of the non-uniform velocity profile at the vena contracta, the "effective" values of C_c used in the momentum and energy relations were not the same. Furthermore, energy losses across the orifice were not negligible, but amounted to 5-7% of the total upstream head. Finally, the discriminant in the equation for t'/B (Appendix 9.1.2.2) was found to be very sensitive to inaccuracies in level measurements, and because it was a small difference of large numbers, it was frequently negative. To make matters worse, the design of the vena contracta level-sensing tap introduced a small velocity head, which produced a systematic error of 0.5 to 0.75 in. in the indicated level measurements; this made it very difficult to check conservation equations or correlate corrections.

The above observations argue in favor of a statistical approach to tie together a body of data consisting of a large number of low-precision measurements. A Froude number polynomial of second order in the dimensionless ratios L_1/B, L_2/B, and $\Delta P_V/B$ obtained by least squares regression has the following desirable properties:

1) A statistically-valid estimate of the associated error can be readily obtained.

2) Since the correlation coefficients are dimensionless, the equation should have good scaleup properties.

3) Although the correlation cannot be safely applied outside the range of the data on which it is based, the use of dimensionless variables serves to compress a large range of physical operating conditions into a small range of dimensionless ratios.

The results of the empirical fit to the submerged-flow data (Figs. 6 and 7) indicate that in this regime Froude numbers increase monotonically with the L_1/B ratio, but that the slope of such a plot is considerably less than that for the non-submerged case. This may mean that the increased baffling effect of submerged discharge decreases the dependence of flow rate on upstream level. Furthermore, as one might expect, Fr_B decreases as L_2/B increases. A larger downstream level would increase t', thus decreasing the rate of flow through the orifice. No explanation is offered for the stronger dependence of Froude number on upstream depth at a $\Delta P_v/B$ of 0.5.

6. CONCLUSIONS

1. Three important classes of single-phase flow occur in a typical evaporator stage.

   a) Shooting flow: no liquid seal is achieved at the outlet weir.

   b) Jump flow: a hydraulic jump occurs on the stage.

   c) Submerged flow: the liquid level behind the inlet weir is higher than the orifice opening.

2. Unsealing and "blow-through" constitute undesirable disturbances which should be avoided for operational stability of an MSF plant.

3. Interstage liquid flow rates may be correlated as

   a) $Fr_B = f'(\frac{L_1}{B}, \frac{\Delta P_v}{B})$ for non-submerged flow.

   b) $Fr_B = f''(\frac{L_1}{B}, \frac{L_2}{B}, \frac{\Delta P_v}{B})$ for submerged flow.

The use of dimensionless ratios allows scaleup of the flow rate relations and increases the range of values of the operating variables spanned by the correlations.

7. RECOMMENDATIONS

1. To develop useful correlations for the position of the hydraulic jump, an apparatus must be constructed to meet the following requirements:

   a) End effects must be eliminated by using at least five experimental stages.

   b) Gas-phase interstage pressure differences must be imposed across both inlet and outlet orifices of the test section.

2. The predicting ability of the flow rate relations developed should be tested against results obtained from experiments on full-scale MSF stages.

3. Since the existence of non-submerged supercritical flow on a stage effectively decreases the interstage coupling, if jump flow could be imposed on every fifth stage for example, a large MSF plant could be broken up into a number of independently controllable sections. This concept should be tested by computer simulation.

8. ACKNOWLEDGEMENT

The authors would like to thank S.J. Ball, N.E. Clapp, Jr., and R.P. Wichner for their help with this project.

9. APPENDIX

9.1 Basic Theory of Open-Channel Flow in an MSF Stage

The following analysis is based upon theoretical considerations given in Refs. (1, 3, 5, and 6).

9.1.1 Non-Submerged Flow

The regimes of shooting flow and jump flow discussed in this report have two important characteristics in common.

1) The regimes are characterized by the presence of a vena contracta in the jet issuing from the bottom of the sluice. This minimum-area section, located about one orifice diameter downstream, must, from continuity considerations, have the greatest average flow velocity, and as a practical matter the distribution of velocities has been found to be nearly uniform.

2) The velocities in the vena contracta region are always greater than the velocities of propagation of small waves on the liquid surface. This relation is expressed as,

$$V/\sqrt{gy} > 1 .$$

The velocity-ratio, $V/\sqrt{gy}$, is normally known as the Froude number, but for purposes of the present report the Froude number will be defined as the square of that ratio, that is, as V^2/gy. At the vena contracta $y = C_cB$, and if the velocity is uniformly distributed, $V = q/C_cB$.

$$\therefore \qquad Fr_{C_cB} = \frac{q^2}{C_c^3 \, gB^3} .$$

Flows for which Fr = 1 are called "cricital;" those for which Fr < 1 and Fr > 1 are denoted as "subcritical" and supercritical," respectively. Thus, in the non-submerged regimes of interest, flow is supercritical.

9.1.1.1 Dimensional Analysis. In non-submerged supercritical flow the effects of downstream disturbances cannot be "felt" at the inlet orifice. Therefore, one would expect to be able to correlate flow rate, q, as a function of the orifice opening, B, the upstream liquid level, L_1, and the interstage pressure difference, ΔP_v. Since gravity is the driving force for flow, the gravitational acceleration constant, g, must also be included. Thus,

$$q = f(B,\ L_1,\ \Delta P_v,\ g)$$

Since this relation involves two fundamental dimensions (length and time) and five variables, Buckingham's π-theorem (7) predicts that the minimum number of dimensionless groups involved is 5 - 2 = 3. The functional relation which may be written is,

$$Fr_B = \frac{q^2}{gB^3} = f'\left(\frac{L_1}{B},\ \frac{\Delta P_v}{B}\right)$$

9.1.1.2 Energy Balance Relationship. In order to elucidate the functional form of the above relationship, an energy balance may be formulated utilizing a control volume which cuts the upstream liquid at (1) and the downstream liquid at the vena contracta (2) (see Fig. 9). If flows are uniform across the cross sections at (1) and (2), conservation of specific energy (7) implies, at steady state,

$$\left(\frac{q}{C_c B}\right)^2 + 2gC_c B = \left(\frac{q}{L_1}\right)^2 + 2g(L_1 + \Delta P_v)$$

or in terms of dimensionless variables,

$$Fr_B = \frac{2C_c^2\left(\frac{L_1}{B}\right)^2\left(\frac{L_1}{B} + \frac{\Delta P_v}{B} - C_c\right)}{\left(\frac{L_1}{B}\right)^2 - C_c^2}$$

This means that,

$$Fr_B = f'\left(\frac{L_1}{B},\ \frac{\Delta P_v}{B}\right)$$

if $C_c = C_c\left(\frac{L_1}{B},\ \frac{\Delta P_v}{B},\ Fr_B\right)$, or $C_c \sim$ constant.

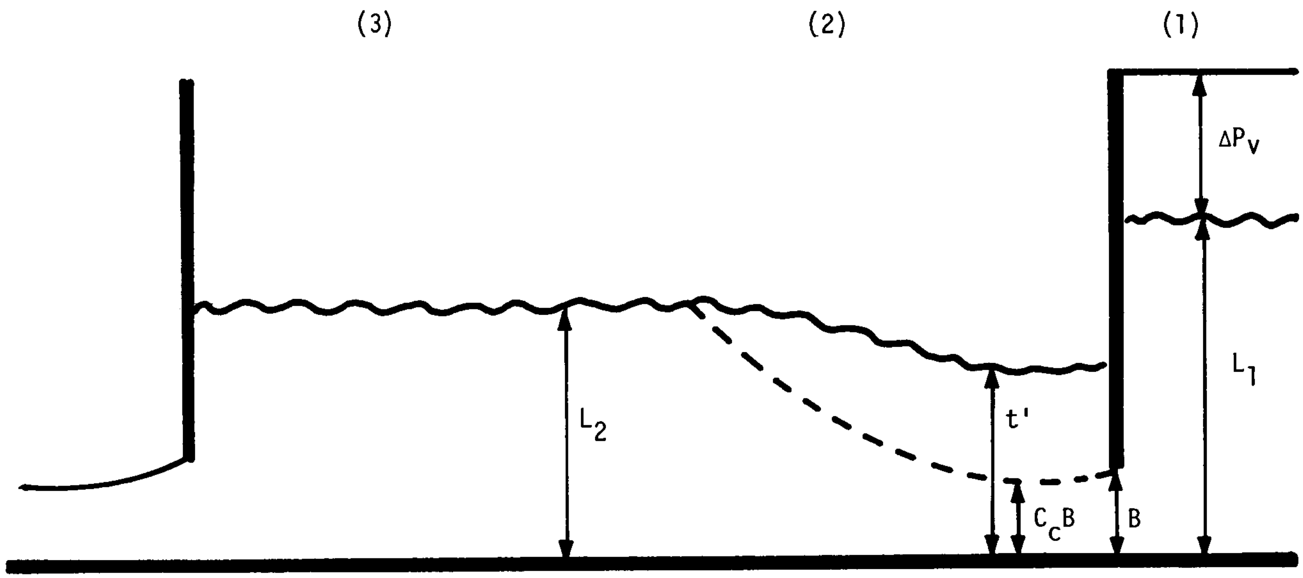

MASSACHUSETTS INSTITUTE OF TECHNOLOGY SCHOOL OF CHEMICAL ENGINEERING PRACTICE AT OAK RIDGE NATIONAL LABORATORY			
Parameters in an MSF Evaporator Stage			
DATE 1-27-70	DRAWN BY TMM	FILE NO. CEPS-X-94	FIG. 9

9.1.1.3 Downstream Momentum Balance. Once the liquid flow rate through the orifice opening is known, it is possible to calculate the liquid level, L_2, on the downstream side of the hydraulic jump from a momentum balance. This has the form,

$$\frac{q^2}{L_2} + \frac{1}{2} g L_2^2 = \frac{q^2}{C_c B} + \frac{1}{2} g C_c^2 B^2$$

or

$$\frac{L_2}{C_c B} = \frac{1}{2} \left(\sqrt{1 + \frac{8 Fr_B}{C_c^3}} - 1 \right)$$

9.1.2 Submerged Flow

The fundamental distinction between non-submerged and submerged flows is that in the latter regime the buildup of a downstream liquid level causes the downstream side of the inlet orifice to be "drowned" or submerged by a level of liquid higher than the orifice opening. The principal effects of submergence are as follows:

1) The level of liquid behind the orifice exerts a net hydraulic head which tends to impede liquid flow through the orifice.

2) Liquid is discharged through the orifice as a submerged turbulent jet, and the liquid velocity may vary from supercritical in the center of the jet to nearly zero at the free surface. The vena contracta is no longer well-defined, since the liquid velocity must "tail off" into the nearly-stagnant region near the surface.

3) There may be greater energy losses due to viscous dissipation in the slowly-circulating liquid above the jet.

9.1.2.1 Dimensional Analysis. Interstage q is now dependent upon an additional parameter: the downstream level, L_2. This adds one additional variable and no additional dimensions, so that

$$Fr_B = f''\left(\frac{L_1}{B}, \frac{\Delta P_v}{B}, \frac{L_2}{B}\right)$$

9.1.2.2 Henry's Equation. The classic analysis of submerged discharge was carried out by Henry (6). This derivation consisted of (Fig. 9):

1) An energy balance across the orifice:

$$\left(\frac{q}{L_1}\right)^2 + 2g(L_1 + \Delta P_v) = \left(\frac{q}{C_c B}\right)^2 + 2gt'$$

2) A momentum balance across the submerged jump:

$$\frac{q^2}{C_c B} + \frac{1}{2}\, g t'^2 = \frac{q^2}{L_2} + \frac{1}{2} g L_2^2 \ .$$

Uniform velocity distributions were assumed at cross sections (1) and (2), and across the vena contracta at (2). The liquid above the vena contracta was considered as stagnant.

Elimination of q^2 gives,

$$\frac{t'}{B} + \frac{K^2 \pm \sqrt{K^4 + 4A\left[A\left(\frac{L_2}{B}\right)^2 - \left(\frac{L_1}{B} + \frac{\Delta P_v}{B}\right) K^2\right]}}{2A}$$

where:

$$A = \frac{1}{4C_c\left(1 - \frac{C_c B}{L_2}\right)}$$

$$K = \frac{1}{\left[1 - \left(\frac{C_c B}{L_1}\right)^2\right]^{1/2}}$$

Then,

$$q = C_c B\, K \sqrt{2g(\Delta P_v + L_1 - t')}$$

9.2 Location of Hydraulic Jump

A control orifice produces supercritical flow downstream and subcritical flow upstream. The orifice in each end of the test stage requires that flow change from supercritical after the inlet to subcritical before the outlet. This transition occurs abruptly at a hydraulic jump. The transition is accompanied by a great deal of turbulence and energy loss. The liquid heights before and after the jump are such that momentum is conserved. In situations where there is little energy loss in all but the jump region, the location of the jump cannot be predicted.

In ducts of uniform cross sections with no slope, energy losses result in a reduction of flow velocity and an increase in flow depth with distance. Since a hydraulic jump can occur only when the liquid depths on either side result in momentum conservation, a depth profile on one or both sides of the jump would have the effect of fixing its location.

In experiments carried out in the test stage it was found that the location of the jump was not random and would move upstream as flow was reduced and downstream as flow was increased. In addition the liquid depths immediately after the jump was observed to be less than the depth further downstream. The existence of the subcritical flow depth profile resulted in a specific location of the jump and explains the movement of the jump location with flow rate. An increase in flow rate increases the momentum of the critical stream and to balance this the jump must move to a location of greater subcritical depth.

An explanation of the depth profile is not obvious. Friction losses due to drag at the walls cannot account for the total energy loss. Other mechanisms such as turbulent rollers and wave motion must contribute. These mechanisms have not been investigated.

9.3 Sample Calculations

9.3.1 Energy Loss

Energy loss across the orifice was computed from the following equation:

$$\Delta E = \left(\frac{g^2}{L_1^2} + 2gL_1\right) - (I_1 - 2gt') \qquad (1)$$

where:

$$I_1 = \frac{\int_o^{t'} V^3\, dy}{\int_o^{t'} V\, dy}$$

The first parenthetical term on the right-hand side is the specific energy upstream of the weir, and the second parenthetical term on the right-hand side is the specific energy at the vena contracta. The t' value used was obtained from momentum conservation over the hydraulic jump. (The experimentally observed t' was not used, as this was subject to error.) The momentum conservation equation is,

$$\frac{1}{2}\, gt'^2 + I_2 = \frac{q^2}{L_2} + \frac{1}{2}\, gL_2^2 \qquad (2)$$

where:

$$I_2 = \int_0^{t'} V^2\, dy$$

The left-hand side of Eq. (2) represents the total momentum flux before the jump and the right-hand side of Eq. (2) the total momentum flux after the jump.

Experimental conditions:

$Q = 2.67\ ft^2/sec$

$L_1 = 16\ in. = 1.33\ ft$

$L_2 = 13.63\ in. = 1.13\ ft$

$B = 9\ in. = 0.75\ ft$

The velocity profile at the vena contracta is shown in Table 2. I_1 and I_2 have been numerically integrated using the velocity profile in Table 3.

Table 2. Velocity Profile at the Vena Contracta

Height from Bottom, y (in.)	Gauge Reading	Velocity, V (ft/sec)	V^2 (ft^2/sec^2)	V^3 (ft^3/sec^3)
0	8.4	4.9	24.1	117.6
1	8.6	5.0	25.0	125.0
2	9.6	5.4	29.2	157.5
3	9.8	5.5	30.2	166.4
4	9.5	5.4	29.2	157.5
4.5	8.4	4.9	24.1	117.6
5	7.0	4.2	17.8	74.1
5.5	5.3	3.2	10.2	32.8
6	4.5	2.6	6.75	17.6
6.5	3.5	1.5	2.25	3.4
7	3.0	0	0	0
8	3.0	0	0	0

Table 3. Numerical Integration of Velocity Profile

Height from Bottom, y (in.)	$\overline{V}\Delta y$ (ft-in./sec)	$\overline{V}^2\Delta y$ (ft^2-in./sec^2)	$\overline{V}^3\Delta y$ (ft^3-in./sec^3)
1	4.95	24.45	121.3
2	5.20	27.10	141.3
3	5.45	29.70	162.0
4	5.45	29.70	162.0
4.5	5.15	26.65	68.8
5	4.55	20.95	47.9
5.5	3.70	14.00	26.7
6	2.90	8.47	12.6
6.5	2.05	4.50	5.3
7	0.7	0.62	0.8
	30.57	148.73	748.7

$$I_2 = \int_o^{t'} V^2\, dy \approx \sum_0^{1.02} \overline{V}^2\, \Delta y = \frac{148.73}{12} = 12.39\ ft^3/sec^2$$

$$I_1 = \frac{\int_o^{t'} V^3\, dy}{\int_o^{t'} V\, dy} \quad \frac{\sum_0^{1.02} \overline{V}^3 \Delta y}{\sum_0^{1.02} \overline{V} \Delta y} = \frac{748.7}{30.57} = 23.5\ ft^2/sec^2$$

Calculation of t' from Eq. (2):

$$\frac{gt'^2}{2} + I_2 = \frac{q^2}{L_2} + \frac{1}{2}\, gL_2^2 = \frac{7.12}{1.13} + 16.1(1.13)^2 = 26.95\ ft^3/sec^2$$

$$\frac{gt'^2}{2} = 26.95 - 12.39 = 14.56\ ft^3/sec^2$$

$$t'^2 = \frac{14.56}{16.10} = 0.903\ ft^2$$

$$t' = 0.95\ ft$$

The measured value of t' was 1.02 ft (error of <7%).

Calculation of energy loss:

Energy upstream of the weir,

$$\frac{q_1^2}{L_1^2} + 2gL_1 = \frac{7.12}{(1.33)^2} + 64.4(1.33) = 4.03 + 85.8 = 89.83\ \frac{ft^2}{sec^2}$$

Energy at the vena contracta,

$$I_2 + 2gt' = 23.5 + 64.4(0.95) = 23.5 + 61.2 = 84.7\ ft^2/sec^2$$

$$\text{percent energy loss} = \frac{89.83 - 84.7}{89.83}(100\%) = \frac{5.1(100\%)}{89.83} = 5.7\%$$

9.3.2 Calculation of Contraction Coefficients

Method 1:

Based on conservation of momentum,

$$C_c = \frac{g^2}{BI_2} = \frac{7.14}{(0.75)(12.39)} = 0.769$$

Method 2:

Based on conservation of energy,

$$C_c = \frac{g}{B}\frac{1}{\sqrt{I_1}} = \frac{2.67}{\sqrt{23.5}(0.75)} = 0.733$$

9.4 Empirical Flow Rate Correlation

The flow rate data of Ball and Clapp (3) were correlated as,

$$Fr_B = f''\left(\frac{L_1}{B}, \frac{L_2}{B}, \frac{\Delta P_v}{B}\right),$$

where the function f" was taken to be a polynomial of second order in each of the three independent variables. The data from 244 flow box runs were fitted by least-squares regression to a polynomial of 27 terms, with a standard error of 4.5%. The polynomial expression was as follows:

with $x = L_1/B$, $y = L_2/B$, $z = \Delta P_v/B$,

$$\begin{aligned} Fr_B = \; & 0.68318 + 0.25914x - 0.22124y + 0.09096z - 0.0055986x^2 \\ & - 0.0028366y^2 - 0.39203z^2 - 0.018233xy - 0.090294xz \\ & + 0.03627yz + 0.010266xy^2 + 0.050509xz^2 + 0.013074x^2y \\ & - 0.26962yz^2 + 0.04527x^2z + 0.064905xyz + 0.028677y^2z \\ & - 0.0043689x^2y^2 + 0.05364x^2z^2 - 0.051734y^2z^2 - 0.014459x^2yz \\ & - 0.0039783xy^2z + 0.075065xyz^2 - 0.010642xy^2z^2 + 0.0078006x^2yz^2 \\ & + 0.00032733x^2y^2z + 0.0029866x^2y^2z^2 \end{aligned}$$

for

$$1.0 < x < 3.4$$

$$1.0 < y < 3.0$$

$$0 < z < 1.3$$

Although the above polynomial is not necessarily the best expansion of the functional relationship, it was adequate to elucidate the various functional dependencies. An expansion in powers of $(L_2/B)^{-1}$ might give a better fit in a smaller number of terms.

9.5 Location of Original Data

The original data for this project are located in ORNL Databook No. A-5510-G, pp. 53-75, on file at the M.I.T. School of Chemical Engineering Practice, Bldg. 1000, ORNL.

9.6 Nomenclature

B orifice opening, ft

C_c contraction coefficient

Fr Froude number, V^2/gy

g gravitational constant, ft/sec^2

L_1 upstream liquid level, ft

L_2 liquid level downstream of the hydraulic jump, ft

ΔP_v interstage pressure difference, ft water

Q liquid flow rate, ft^3/sec

q liquid flow rate per unit width of channel, ft^2/sec

t' liquid level at the vena contracta for a submerged flow, ft

V liquid flow velocity, ft/sec

y height of liquid, in.

Also, see Fig. 7.

9.7 Literature References

1. Ball, S.J., N.E. Clapp, B. Squires, and R. Van Winkle, "Dynamics Experiments on the AMF Millstone Point Flash Evaporator," ORNL-TM-2188, pp.45-48 (1968).

2. Clapp, N.E., Jr., personal communication, ORNL, January 19, 1970.

3. Chow, Ven Te, "Open Channel Hydraulics," 1st ed., pp. 393-434, McGraw-Hill, New York (1959).

4. Hammond, R.P., "Nuclear Desalination Program Report on Activities of Interest to Atomic Energy Commission," ORNL-CF-69-9-7, pp. 4-7 (1969).

5. Henderson, F.M., "Open Channel Flow," 1st ed., pp. 202-210, Macmillan Co., New York (1966).

6. Henry, H.R., "Discussion of Paper by M.L. Albertson, Y.B. Dai, R.A. Jensen, and H. Rouse, 'Diffusion of Submerged Jets,'" Trans. Am. Soc. Civil Eng., 115, 639-697 (1950).

7. Vennard, J.K., "Elementary Fluid Mechanics," 4th ed., pp. 348-392, John Wiley & Sons, New York (1962).

INTERNAL

1. T.D. Anderson
2-4. S.J. Ball
5. N.E. Clapp, Jr.
6. J.G. Delene
7. R.P. Hammond
8. W.H. Kelley, Jr.
9. Lewis Nelson
10. L.C. Oakes
11. I. Spiewak
12. R.S. Stone
13. R. Van Winkle
14. R.P. Wichner
15-16. Central Research Library
17. Document Reference Section
18-20. Laboratory Records
21. Laboratory Records, ORNL R.C.
22. ORNL Patent Office
23-37. M.I.T. Practice School

EXTERNAL

38. R.F. Baddour, MIT
39. L.B. Evans, MIT
40. S.M. Fleming, MIT
41. E.R. Gilliland, MIT
42. H.C. Hottel, MIT
43. T.W. Kerlin, UT
44. S.T. Mayr, MIT
45. H.S. Mickley, MIT
46. C.F. Moore, UT
47. J.C. Robinson, UT
48. A.F. Sarofim, MIT
49. K.A. Smith, MIT
50. P.S. Virk, MIT